FLEXIBLE WINGS FOR HARVESTING AND STORING SOLAR ENERGY IN UNMANNED AIR VEHICLES

Alex Holness[1], Lena D. Johnson[2], Hugh A. Bruck[3] and Satyandra K. Gupta[4]

[1] Department of Mechanical Engineering
University of Maryland, College Park, MD 20742
Email: holness1@umd.edu

[2] Department of Mechanical Engineering
University of Maryland, College Park, MD 20742
Email: ldj556@gmail.com

[3] Department of Mechanical Engineering
University of Maryland, College Park, MD 20742
Email: bruck@umd.edu

[4] Aerospace and Mechanical Engineering
University of Southern California
Email: guptask@usc.edu

Keywords: Flexible Multifunctional Wings, Flexible Solar Cells, Flexible Batteries, Unmanned Air Vehicles, Flight Time

ABSTRACT

Flexible energy harvesting/storage components are being used on Unmanned Air Vehicles (UAVs) to increase operational performance, particularly to increase flight time. We have developed highly compliant, multifunctional composite structures for the wings of a novel flapping wing UAV platform known as "Robo Raven", using a new layered manufacturing technique. Robo Raven is capable of flight using just flapping or in a mixed-mode using flapping and conventional propellers. Changes in the aerodynamic loads were characterized throughout the flapping cycle to understand the effects of integrating the flexible energy harvesting/storage materials on wing mechanics. Both aerodynamic and multifunctional performance models were developed to understand how integration of flexible solar cells and flexible batteries into the wings influences flight performance, in particular flight endurance. Multifunctional wing structures with mass simulating the energy harvesting/storage structures were compared with both regular wings and previously developed multifunctional wings with flexible solar cells. Fitting the models to the experimental data to determine the modeling parameters, it was possible to predict flight gains of up to 40% at the maximum flight time of 4 Hz for all of the multifunctional wing structures over the regular wings.

1 INTRODUCTION

As Unmanned Air Vehicle (UAV) technology continues to expand, bio-inspired UAV technology is increasingly pushing the boundaries of function and design; becoming increasing similar in construct to the their natural source of inspiration [1]. At the same time, as UAV applications grow increasingly diverse, enhancing the multi-functionality of materials and structures that are used are becoming critical to optimizing flight performance, particularly time of flight. However, there exists a trade-off between the added technical capabilities of multifunctional design and the increased aerodynamic capabilities of bio-inspiration.

UAV emulation and reproduction of nature's flying mechanisms have come in a variety of forms. There exist platforms that have been designed to increase aerodynamic performance by

replicating the morphing wing capabilities of bats and birds. For example, Grant's [2] multi-joint and gull-wing morphing platforms characterised different mechanisms of morphing. Furthermore, Ijfu's [3] latex rubber morphing wing displayed the ability to change shape in accordance with wind speed. Methods such as this, feature either an active morphing of the wing's structure through a form of actuation, or passive morphing of the wing through compliant structures. Other platforms seek to generate aerodynamic forces and increase performance through flapping wing flight. These platforms, named "ornithopters", generate propulsion and lift through bird-like flapping wings. The performance characteristics of these platforms may be modified through the change of flapping frequency, control of a tail, and the efficiency of the actuators that provide propulsion. Examples of this include the University of Maryland's Robo Raven, Small Bird, and Big Bird platforms [4,5], the Delfly [6], Bat Bot [7]and the Nano Hummingbird [8].

Finally, there has been countless research efforts to improving lift and thrust generation through the inclusion, characterization and modification of an airfoil [9]. The leading edge of a bird's wing possesses an airfoil-like profile that differs in geometry depending upon the species of bird. Furthermore, there is a correlation between the shape of a bird's airfoil and its primary flying characteristics [4 10]. Airfoils have been integrated into fixed-wing UAV design since their inception [10]. However, even as UAV's advance in performance through the methods discussed above, nature's fliers continue to possess a level of aerodynamic performance and flight efficiency that is currently unmatched by any UAV, or other aircraft, platform [10,11].

The University of Maryland's Robo Raven platform seeks to increase aerodynamic performance of UAVs through more controlled lift and thrust generation using multifunctional wings with integrated energy capture and storage elements, such as solar panels [12], and compliant bio-inspired geometries [13] that can morph to improve the duration or aerobatic performance using either flapping or mixed-mode flight consisting of flapping and conventional propeller-driven propulsion [28]. However, the introduction of additional elements into the wings can decrease flexibility, resulting in decreased generation of lift and thrust. Previously, detrimental effects of adding energy capture elements to the flexible wings of Robo Raven has been shown to be mitigated by proper preparation and placement of these elements, as well as slight redesign of the wing shape [12]. However, there has been no research on the inclusion of a flexible battery element into the wings, with or without the flexible solar cells.

In this paper, the effects of integrating energy capture and storage elements into flexible wings for prolonging flight of UAVs, such as Robo Raven, are investigated. This research was not only undertaken to improve the platform's aerodynamic performance, but also to better understand the implications of increasing weight and stiffness of the wing through the integration of multifunctional components. The aerodynamic forces associated with the change of weight and stiffness of the wing are experimentally characterized over a range of flapping frequencies. New models for the aerodynamic performance of the multifunctional wings, as well as the system performance with the actuator that controls their position and their subsequent multifunctional performance, are also developed to predict the subsequent payload capacity of the UAV, and the associated flight time by determining the modelling parameters from fits to the experimental data.

2 DESIGN AND MANUFACTURE OF FLEXIBLE MULTIFUNTIONAL WINGS

Robo Raven is a flapping wing UAV with bird-like, body geometry and independent wing control (Figure 1). It is capable of flight by just flapping the wings (Robo Raven I viewed in flight at https://www.youtube.com/watch?v=mjOWpwbnmTw), or in a mixed-mode by flapping the wings and using propellers (Robo Raven V viewed at https://www.youtube.com/watch?v=Yryz8PSAwmA) [4, 28]. Its wings are made of I mil thick flexible mylar sheets and carbon-fiber spars. An schematic of the wing design can be seen in Figure 2. The wings are manufactured using a layered Additive Manufacturing (AM) process that has been more thoroughly examined in previous papers [4, 5]. This process allows for the creation of a lightweight wing with variable wing design parameters (seen in Figure 2), with few manufacturing steps. The carbon-fiber spars provide stiffness and stability to the wing so that it might maintain an advantageous shape during both the downstroke and upstroke of the flapping cycle. The front carbon-fiber rod is the thickest and provides both attachment to the platform's body and stability of the wing shape. Cross-spars prevent an unfavourable torque in the wing during

flapping, but are flexible enough to deform upwards and downwards during the apex and nadir of the flapping stroke (Figure 2). The trailing edge of the wing is left to freely deform to generate more thrust through the blow back effect. The wings are driven by Futaba S bus S9372SV servos with a maximum torque of 24.6 N-cm and maximum angular speed of 1000 deg/sec.

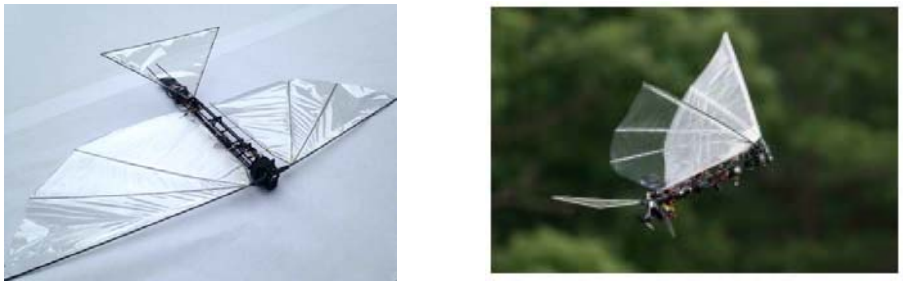

Figure 1. (left) Robo Raven I with just flapping mode [4], and (right) Robo Raven V with mixed-mode [28].

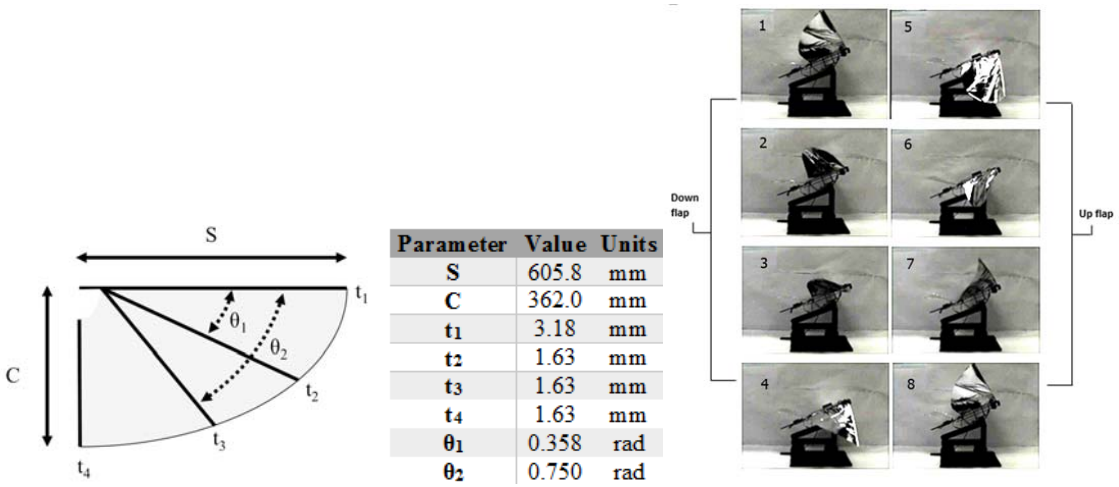

Parameter	Value	Units
S	605.8	mm
C	362.0	mm
t_1	3.18	mm
t_2	1.63	mm
t_3	1.63	mm
t_4	1.63	mm
θ_1	0.358	rad
θ_2	0.750	rad

Figure 2. (left) Robo Raven I wing design, (center) typical design parameters for the wing, and (right) deformation of wing during flapping [4].

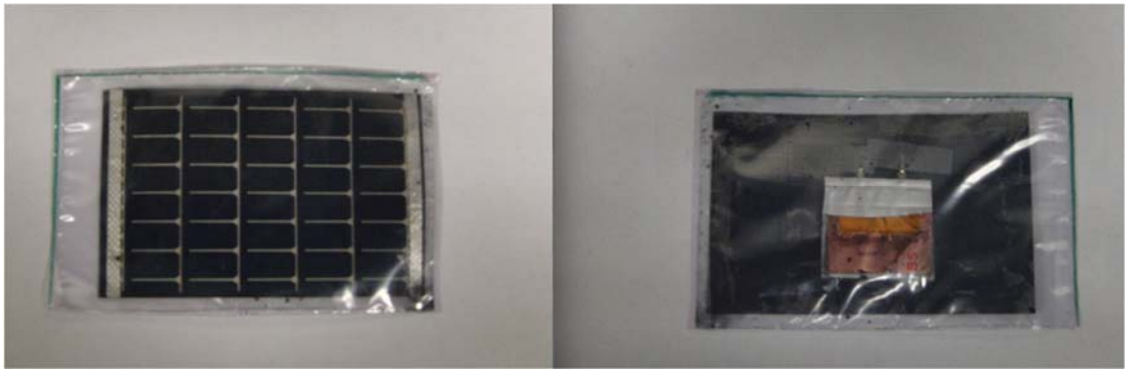

Figure 3. A picture of the battery-solar packets, (Left) from the top, (Right) from the bottom.

Solar-battery packs were created to add energy capture and storage elements to the wing (Figure 3). To create the packs, flexible amorphous silicon Powerfilm MPT6-75 flexible solar cell modules with

dimensions 0.2 mm thick x 7.3 cm x11.4 cm and 0.3 W output were used by delaminating their protective plastic encapsulation to substantially increase their flexibility and reduce the areal density to 0.02 g/cm^2. Flexible thin LiPo batteries with dimensions 0.5 mm thick x 43 mm x 38 mm with 50 mAh capacity were also put through a delamination process to increase their flexibility and reduce areal density to 0.104 g/cm^2. This was accomplished by cutting away the front outer casing to reveal the inner components. The battery was attached to the back of the solar panel and impulse sealed into a PET plastic coating. These battery packs were then integrated into the wing with the layered AM process. A resulting multifunctional wing can be seen in Figure 4 with three solar-battery packs were attached to the upper portion of the wing at the leading edge. In addition to the energy harvesting materials, the effects of these materials on aerodynamic performance were simulated using 3 mil laminated sheets with an areal density of 0.019g/cm^2.

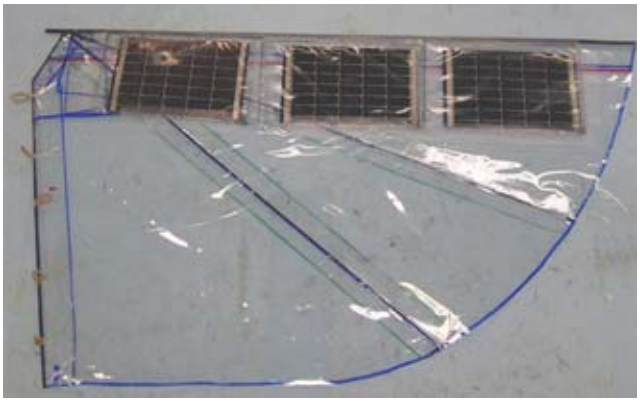

Figure 4. Multifunctional wing with 3 integrated battery/solar cell module packages at leading edge.

3 MATHEMATICAL MODELING OF PERFORMANCE

3.1 AERODYNAMIC PERFORMANCE

A mathematical model was used to describe and quantify the possible aerodynamic performance of the different wing types created for testing. During flapping flight, thrust and lift undergo periodic, yet inconsistent, variations. A common modelling approach is to use a quasi-steady state assumption [14,15]. Quasi-steady state wing theory assumes that the forces on a moving wing are equivalent to the sum of the forces on a fixed wing over a sequence of attitudes that track the wing motion. This model neglects acceleration forces and unsteady aerodynamics effects [16,17]. In very small intervals of time, the flight is considered level with no acceleration. This implies that the forces in all directions must be equal during steady state flight, assuming no change in mass.

Forces must sum to zero to maintain level, steady and un-accelerated flight along the vertical. Assuming no loss of mass or body forces aside form gravity for steady state flight conditions, the lift force, F_1, must offset the weight, W = mg, as follows [18].

$$F_L = mg \tag{1}$$

The aerodynamic lift is given by:

$$F_L = \frac{1}{2}\rho S V^2 C_L \tag{2}$$

Where C_L is the coefficient of lift, ρ is the density of air, S is the planform area, and V is the forward velocity. Substituting Equation (2) into Equation (1) yields:

$$\frac{1}{2}\rho S V^2 C_L = mg \tag{3}$$

In the horizontal direction, the thrust force, F_T, must be equal to the drag force, F_D, during steady state flight:

$$F_T = F_D \tag{4}$$

where the drag force is defined using the coefficient of drag, $C_{n,p}$:

$$F_D = \frac{1}{2}\rho V^2 S C_{D,p} \tag{5}$$

Substituting Equation (5) into Equation (4) yields:

$$F_T = \frac{1}{2}\rho V^2 S C_{D,p} \tag{6}$$

A proposed flapping wing model for the thrust is the following:

$$F_T = k_F f^2 S \Delta\alpha \tag{7}$$

This is produced with insight gained from [19] which notes that thrust increases with flapping frequency, f, and amplitude of oscillation. An advance ratio, J, was previously defined for Flapping Wing Aerial Vehicles (FWAVs) as follows [15,20,21,22]:

$$J = \frac{V}{2\Delta\alpha f b} \tag{8}$$

where b is the wing span.

Since it is possible to relate thrust to lift using the velocity, Equation (6) can be rearranged, and solving for V^2 yields:

$$V^2 = \frac{2F_T}{\rho S C_{D,p}} \tag{9}$$

Substituting Equation (9) into Equation (6) yields:

$$F_L = \frac{C_L}{C_{D,p}} F_T \tag{10}$$

Because the average thrust is generated using the flapping wings. Substituting the thrust generated by flapping (Equation (7)) into Equation (10) results in:

$$F_L = \frac{C_L}{C_{D,p}} k_f f^2 S \Delta\alpha \tag{11}$$

Substituting the lift into Equation (3) yields the maximum flight weight for a FWAV, as follows:

$$\frac{C_L}{C_{D,p}} k_f f^2 S \Delta\alpha = mg \tag{12}$$

Thrust governs the offsetting drag force value by dictating the velocity in the relationship given in Equation (6) (if all else remains constant). An increase in velocity benefits lift generation by way of aerodynamic lift, as seen in Equation (2). Given this, thrust and lift are directly related via their drag

coefficients, as seen in Equation (10). These relationships provide insight into ways to increase performance by increasing thrust production in a FWAV.

3.2 MULTIFUNCTIONAL PERFORMANCE

Furthermore, it was important to create a model to represent the flight time improvements that might be made by adding a solar-battery pack to the wing. When operating on a battery only, Robo Raven's flight time, t_f, can be determined as follows:

$$t_f = \frac{E_a}{P_c} \tag{13}$$

where P_c is the average power consumed over a flapping cycle, and E_a is the energy available. The energy available is a function of the battery mass, M_b, and its specific energy, β, as follows:

$$E_a = \beta M_b \tag{14}$$

The upper limit of the on board energy source mass is limited by the amount of mass that can be carried (i.e., the payload capacity). Though the quasi steady state assumption is simplistic and does not always predict flapping flight performance it is a helpful first order approximation and it is a common approach to use it [14]. Using the quasi-steady state assumption, for level flight where the acceleration is equal to zero, the maximum flight mass, M_{max}, must be equal to the total lift mass that can be carried:

$$M_L = M_{max} \tag{15}$$

Using Equation (12):

$$M_L = \frac{\frac{C_L}{C_{D,p}} k_f f^2 S \Delta\alpha}{g} \tag{16}$$

Therefore, the payload, M_{pl}, is determined from the base platform mass, M_{FWAV} , as follows:

$$M_{pl} = \frac{\frac{C_L}{C_{D,p}} k_f f^2 S \Delta\alpha}{g} - M_{FWAV} \tag{17}$$

The limit to the amount of power source mass is determined by the payload:

$$M_b = M_{pl} \tag{18}$$

The flight time then becomes

$$t_f = \frac{\left(\frac{\frac{C_L}{C_{D,p}} k_f f^2 S \Delta\alpha}{g} - M_{FWAV}\right) * \beta}{P_c} \tag{19}$$

In depletion, the net consumed power is then the difference between the power consumed by the motors and the powers provided by the solar cells.

$$P_c = P_{Motor} - P_{Solar} \tag{20}$$

Therefore:

$$t_f = \frac{\left[\frac{\frac{C_L}{C_{D,p}} k_f f^2 S\Delta\alpha}{g} - M_{FWAV} + (\rho_{sc+b} - \rho_w) * A_w\right] * \beta}{P_{Motors} - P_{Solar}} \quad (21)$$

Where ρ_{sc+b} is the areal density of the flexible solar cells and flexible batteries, and ρ_w is the density of the wing material. Equation (21) now represents the model of multifunctional performance that can be used to gauge the trade off in the physical and electrical characteristics of the solar cells, as well as the effects of the multifunctional wings on the flapping mechanics of the FWAV. It is important to note that the power generation from the solar cells and the consumption of the motors driving the wings wary as a function of time. In the case of the solar cells the power curve has a relationship between voltage and current as given in Fig. 14. As a result of the nature of the circuit, the power draw from the solar cells may vary due to changes in voltage from the servos and batteries. The use of a maximum powerpoint tracking unit can minimize this effect, but it will add additional mass to the system and is not 100% efficient. Therefore, we assessed the effects of integrating the solar cells from direct measurements of the power draw as a function of flight time.

3.3 WING-MOTOR SYSTEM PERFORMANCE

In addition to the aerodynamic and multifunctional considerations, the actual wing performance will also be controlled by the motor characteristics. Specifically, the servo motors have the following attributes:

$$P_{draw} = P_{max}\,(1-\omega/\omega_{max}) \quad (22)$$

$$T = T_{max}\,(1-\omega/\omega_{max}) \quad (23)$$

where P_{draw} is the power draw, T is the torque, and ω is the angular speed. The torque will dictate the amount of aerodynamic force that can be generated, since it is opposed by the drag force of the flapping wing that deforms the wing to generate the thrust. It is important to note that the available torque to power to generate the thrust may be further reduced by the weight of the wing, $m_w g$, and the center of mass, d. Therefore, it is possible to approximate the desired thrust output as being proportional to the torque output as follows:

$$F_T = k_1(T+sgn(T)m_w g d) \quad (24)$$

Therefore, we can see from Equation (7) and noting that $4f\Delta\alpha=\omega$, the following condition must hold for the wing to flap at the desired frequency and amplitude:

$$k_F f^2 S\Delta\alpha < k_1[T_{max}(1 - 4f\Delta\alpha/\omega_{max}) + sgn(T)m_w g d)] \quad (25)$$

Therefore, it is possible to determine the frequency at a given amplitude that is necessary to generate the maximum thrust for a given wing design as follows:

$$f=(-4k_1T_{max}\Delta\alpha/\omega_{max}+[16(k_1T_{max}\Delta\alpha/\omega_{max})^2+4k_FS\Delta\alpha k_1(T_{max}+sgn(T)m_w g d]^{1/2})/(2k_FS\Delta\alpha) \quad (26)$$

Neglecting the mass effect of the wing, it can be seen that as $\Delta\alpha >> k_F\omega^2_{max}S/(4T_{max}k_1)$:

$$f = \omega_{max}/(4\Delta\alpha) \quad (27)$$

and the subsequent torque generation approaches 0, which does not result in flight. Likewise, as $\Delta\alpha << k_F\omega^2_{max}S/(4T_{max}k_1)$:

$$f^2 = k_1 T_{max}/(S k_F \Delta\alpha) \quad (28)$$

and the subsequent torque can approach T_{max} at very high frequencies (like a hummingbird). Given the frequency and amplitude, it is then possible to determine the power required to achieve that thrust from Equation (31). This in turn can be used in Equation (30) to determine the flight time. Thus, an optimal flapping frequency and amplitude can be determined f multifunctional or the wings.

4 TESTING PROCEEDURES

In order to assess the aerodynamic performance of the multifunctional wings, a static testing platform was previously created (Figure 5). This test stand was statically mounted to a test stand equipped with an American Digital E5 optical encoder to record the wing flapping amplitude, and an ATI Mini40 six-axis force/torque transducer. Thrust measurements were recorded in 5 m/s (as measured by a pitot tube) of airflow generated by fan in a wind tunnel [5]. The force transducer is capable of independently measuring all six components of force and torque using a Cartesian coordinate system and was calibrated by ATI to measure up to 40 N in the X and Y directions with a resolution of 1/100 N (1.02 g) of resolution and 120 N in the Z direction with a resolution of 1/50 N (2.04 g). The resonant frequency for Fx, Fy, and Fz measurements are 3200 Hz, which is far beyond the operating frequency. This test stand design was developed and utilized in previous flapping flight work [23] and has characterized Robo Raven in previous work [4 5 26 27]. Similar approaches with load cells have been used in other flapping research work [24].

Figure 5. (left) Test stand created for characterizing Robo Raven's wings, and (right) ATI Mini40 six-axis force/torque transducer used to record aerodynamic forces.

Data was recorded using a LabView VI interfaced with a National Instruments data acquisition system after the static platform was mounted on the load cell. During operation, the data was gathered for 5 seconds at 1,000 samples per second. The flapping was started and stopped before and after each capture window to ensure well-developed operation free of initial and final transients. These 5,000 samples were then averaged to provide the net thrust. The test was then repeated two more times. The average of three trials was then averaged produce the final figure for thrust provided. To prevent issues with motor heating which could skew the results, time was allowed between tests.

5 EXPERIMENTAL AND MODELLING RESULTS

To understand the effects of salient characteristics, such as changes in mass and stiffness, of the multifunctional wing design on the multifunctional performance, and to determine the validity of the model, the following wing designs were tested:

1. Regular Robo Raven 1 wing (0.164 m^2 in area with a span of 0.55 m, a 0.325 m chord, and 16.3 g total mass)

2. Regular wing with 3 layers of 15 cm x 20 cm rectangular piece of substantially stiffer 3 mil thick lamination sheet (5.8 g) simulating energy storage/harvesting material on the leading edge near the root of the wing (Figure 6).
3. Regular wing with 3 layers of 15 cm x 20 cm rectangular piece of 3 mil thick lamination sheet (5.8 g) simulating energy storage/harvesting material on the trailing edge of the wing.
4. Regular wing with 11 Powerfilm flexible solar cell modules covering most of the wing and adding an additional 18.3 g of mass (Figure 6).
5. Regular wing with 3 flexible LiPo battery+Powerfilm solar cell modules at the leading edge of the wing (Figure 4).

Aerodynamic results from testing the wings on the stand at a programmed flapping amplitude of 50^o (the maximum that can be tested without the wings touching the bottom of the stand) can be seen in Figure 7. The encoder-measured flapping range (i.e., twice the flapping amplitude) was plotted against flapping frequency, and the residual thrust with the wind tunnel at a speed of 6 m/s is plotted against flapping frequency. Also shown are the modeling fits obtained from Equations (7) and (26) for the thrust and flapping angle respectively can also be seen. In these fits, there was not substantially different between the regular wings and the substantially stiffer lamination film on the trailing and leading edge. However, the solar cells did show some effect on the flapping angle due to an increase in the drag by 150% from the solar cell stiffness and mass, however there was no significant effects on the residual thrust measurements. This is likely due to additional deformation of the trailing edge that allows for more air to be displaced. he multifunctional wings with the flexible LiPo batteries and flexible solar cells at the leading edge produced nearly identical performance as the solar cell wings, having less stiffness near the trailing edge, more stiffness at the leading edge, and about 50% less additional mass.

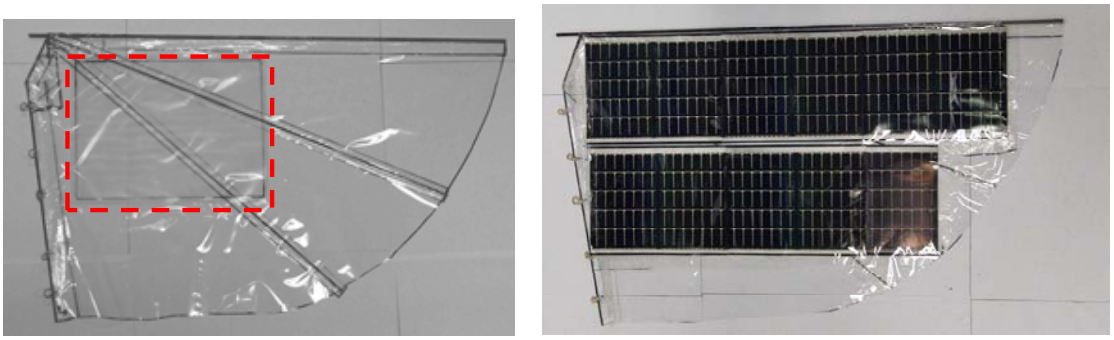

Figure 6. Regular wing with (left) the 3 mil laminated film at leading edge outlined in red, and (right) 11 Powerfilm MPT6-75 flexible solar cell modules covering most of the wing.

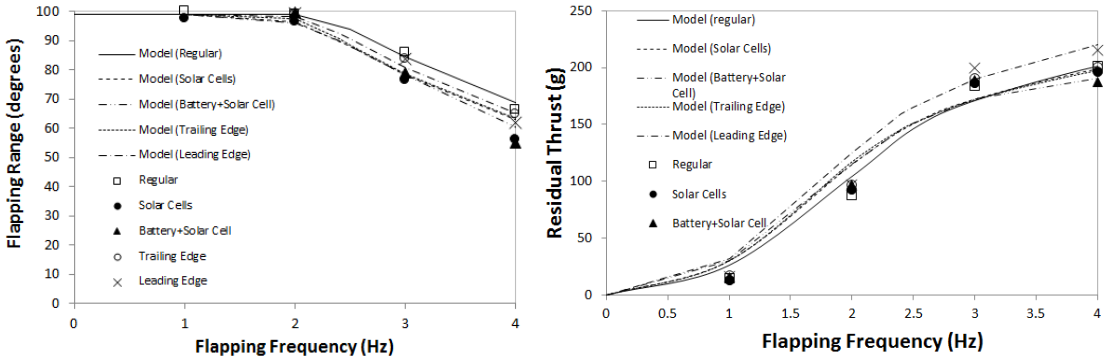

Figure 7. (left) Measured changes in flapping angle with flapping frequency and fits from Equation (26) for the 4 different wing designs, and (right) change in the associated residual and fits from Equation (7).

The implications of the aerodynamic testing results and modeling on power and multifunctional performance can be seen in Figure 8. The power draw can now be determined from the calculated torque loading at each frequency, and the inherent efficiency of the motor at each frequency. The multifunctional performance model prediction of flight time, Equation (21), can now be used to predict the flight time using LiPo batteries with a typical storage capacity of approximately 352 J/g. It can be seen that this particular solar wing configuration can provide a flight time improvement of 20% at 4 Hz, where the maximum flight time occurs, as previously reported [12,17]. The multifunctional wings with flexible LiPo batteries and flexible solar cells at the leading edge is predicted to have a 40% improvement in flight time benefit. An improvement of 35% is also predicted at 4 Hz when the mass in the simulated wings is at the leading edge and assumed to be flexible LiPo battery material. Thus, this modeling has the potential for determining the benefits of using flexible energy storage/harvesting materials in multifunctional wings for flapping wing UAVs.

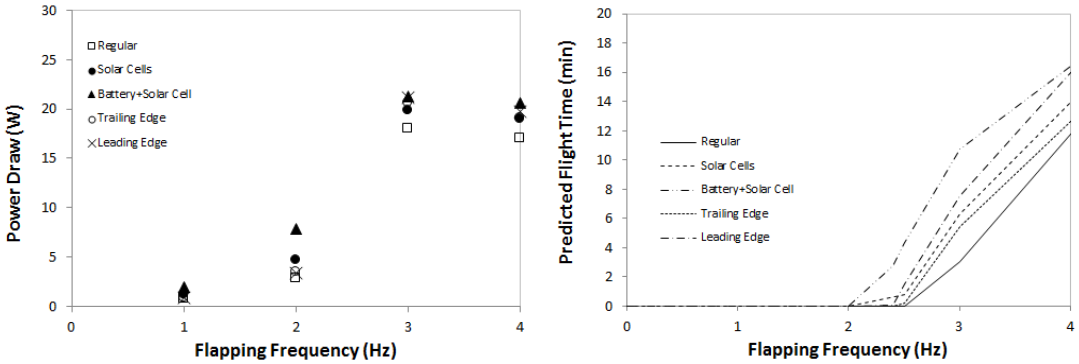

Figure 8. (left) Power draw for each wing for a single servo, and (right) predicted flight time for each flapping condition from multifunctional performance model from Equation (21).

6 CONCLUSIONS

Flexible energy harvesting/storage components have been used to create multifunctional wings for flapping wing UAVs to increase operational performance, particularly to increase flight time. Highly compliant, multifunctional composite structures for the wings of a novel flapping wing UAV platform known as "Robo Raven", were realized using a new layered manufacturing technique. Changes in the aerodynamic loads were characterized throughout the flapping cycle to understand the effects of integrating the flexible energy harvesting/storage materials on wing mechanics. Both aerodynamic and multifunctional performance analyses were developed to understand how integration of flexible solar cells and flexible batteries into the wings influences flight performance, in particular flight endurance. Multifunctional wing structures with mass simulating the energy harvesting/storage structures were compared with both regular wings, the new multifunctional wings with flexible LiPo batteries and flexible amorphous silicon solar cells, and previously developed multifunctional wings with flexible amorphous silicon solar cells. Fitting the models to the experimental data to determine the modeling parameters, it was possible to predict flight gains of up to 40% at the maximum flight time of 4 Hz for all of the multifunctional wing structures over the regular wings.

ACKNOWLEDGEMENTS

This work was sponsored by AFOSR grant FA9550-15-1-0350 with Dr. Byung-Lip "Les" Lee program manager. Opinions expressed are those of the authors and do not necessarily reflect opinions of the sponsors.

REFERENCES

[1] A. Perez-Rosado, A. E. Holness, H.A. Bruck, and S.K. Gupta, Multifunctional compliant wings to harvest solar energy in flapping wing aerial vehicles, *Proceedings of the 21th International Conference on Composite Materials, Xi'an, August 20-25 August, 2017*.

[2] D. T. Grant, M. Abdulrahim, and R. Lind, Flight dynamics of a morphing aircraft utilizing independent multiple-joint wing sweep, *International Journal of Micro Air Vehicles, 2(3):91-106.* 2010.

[3] P. G. Ifju, D. A. Jenkins, S. Ettinger, Y. Lian, and W. Shyy, Flexible-wing-based micro air vehicles, *40th AIAA Aerospace Sciences Meeting & Exhibit.* 2002.

[4] J. W. Gerdes, A. Holness, A. Perez-Rosado, L. Roberts, A. Greisinger, E. Barnett, J. Kempny, D. Lingham, C. Yeh, H. A. Bruck, and S. K. Gupta, Robo Raven: a flapping wing air vehicle with highly compliant and independently controlled wings, *Soft Robotics, 1(4):275-288.* 2014.

[5] J.W. Gerdes, S.K Gupta, and S. Wilkerson, A Review of Bird-Inspired Flapping Wing Miniature Air Vehicle Designs, *ASME Journal of Mechanism and Robotics*, *4(2).* 021003.1-021003.11. 2011

[6] A. Ramezani, X. Shi, S. Chung, and S. Hutchinson. Bat bot (B2), a biologically inspired flying machine. *In IEEE International Conference on Robotics and Automation, May 2016*

[7] G. de Croon, K. de Clercq, r. Ruijsink, B. Remes, and C. de Wagter, Design, aerodynamics, and vision-based control of the Delfly, *International Journal of Micro Air Vehicles, 1(2):71-97.* 2009.

[8] M. Keennon, K. Klingebiel, H. Won, and A. Andriukov, Development of the nano hummingbird: a tailless flapping wing micro air vehicle, *50th AIAA Aerospace Sciences Meeting Including the New Horizons Forum and Aerospace Exposition, Nashville, January, 9-12, 2012.*

[9] W.B. Tay, and K.B. Lim, Analysis of non-symmetrical flapping airfoils, *Acta Mech Sin,* 2009.

[10] D. E. Alexander, *Natures flyers: birds, insects, and the biomechanics of flight.* Baltimore, MD: Johns Hopkins University Press, 2002.

[11] T. J. Mueller, *Fixed and flapping wing aerodynamics for micro air vehicle applications.* Reston, VA: American Institute of Aeronautics and Astronautics, 2001.

[12] A. Perez-Rosado, R. D. Gehlhar, S. Nolen, S. K. Gupta, and H. A. Bruck, Design, fabrication and characterization of multifunctional wings to harvest solar energy in flapping wing air vehicles, *Smart Materials,24(6).* 2015.

[13] C. H. Jenkins, *Compliant structures in nature and engineering*, Boston, MA, 2005.

[14] T. Mueller, and J. DeLaurier, Aerodynamics of small vehicles, *Annual Review of Fluid Mechanics,35:89-111. 2003.*

[15] W. Shyy, H. Aono, C. K.Kang, and H. Liu. *An Introduction to Flapping Wing Aerodynamics*. Cambridge University Press, 2013. Cambridge Books Online.

[16] F.T. Muijres, LC Johansson, Ryan Barfield, Marta Wolf, GR Spedding, and Anders Hedenstr¨om. Leading-edge vortex improves lift in slow-flying bats. *Science*, 319(5867):1250–1253, 2008.

[17] R. Madangopal, Z. A. Khan, and S. K. Agrawal. Biologically inspired design of small flap ping wing air vehicles using four-bar mechanisms and quasi-steady aerodynamics, Journal of Mechanical Design, 127(4):809–816, 2004.

[18] J. D. Anderson. *Introduction to Flight*. McGraw Hill, New York, NY, 7 edition, 2012.

[19] M. F Platzer, K.D. Jones, J. Young, and J.C.S. Lai. Flapping wing aerodynamics: progress and challenges, *AIAA journal, 46(9):2136–2149, 2008.*

[20] W. Shyy, M. Berg, and D. Ljungqvist. Flapping and flexible wings for biological and micro air vehicles, *Progress in Aerospace Sciences, 35(5):455 – 505, 1999.*

[21] S. Ho, H. Nassef, N. Pornsinsirirak, Y.-C. Tai, and C.-M. Ho. Unsteady aerodynamics and flow control for flapping wing flyers, *Progress in Aerospace Sciences, 39(8):635–681, 2003.*

[22] L. Zhao, Q. Huang, X. Deng, and S.P. Sane. Aerodynamic effects of flexibility in flapping wings, *Journal of The Royal Society Interface, August 2009. 10.1098/rsif.2009.0200.*

[23] D. Mueller, H.A. Bruck, and S. K. Gupta. Measurement of thrust and lift forces associated with drag of compliant flapping wing for micro air vehicles using a new test stand design, *Experimental Mechanics, 50(6):725 – 735, 2010.*

[24] C. Rose and R.S. Fearing. Comparison of ornithopter wind tunnel force measurements with free flight, *In Robotics and Automation (ICRA), 2014 IEEE International Conference on, pages 1816–1821, May 2014.*

[25] A. Perez-Rosado, H. Bruck, and S. K. Gupta. Integrating solar cells into flapping wing air vehicles for enhanced flight endurance. *Journal of Mechanisms and Robotics, 8:051006–1, 2016.*

[26] A Perez-Rosado, G.J. Griesinger, H.A. Bruck, and S. K. Gupta. Performance characterization of mul- tifunctional wings with integrated solar cells for miniature air vehicles. *In ASME IDETC/CIE, 38th Mechanisms and Robotics Conference. ASME, August 2014. DETC2014-34719.*

[27] A. Perez-Rosado, H.A. Bruck, and S. K. Gupta. Enhancing the design of solar-powered flapping wing air vehicles using multifunctional structural components. *In ASME IDETC/CIE, 39th ASME Mechanism and Robotics Conference, pages V05BT08A016–V05BT08A016. ASME, August 2015. DETC2015-47570.*

[28] A.E. Holness H.A. Bruck, and S. K. Gupta. Design of Propeller-Assisted Flapping Wing Air Vehicles for Enhanced Aerodynamic Performance. *In ASME IDETC/CIE, 39th ASME Mechanism and Robotics Conference, pages V05BT08A016–V05BT08A016. ASME, August 2015. DETC2015-47577.*